

Laser accelerated heavy particles – Tailoring of ion beams on a nano-scale

M. Roth ^{a,*}, P. Audebert ^b, A. Blazevic ^c, E. Brambrink ^b, J. Cobble ^d, T.E. Cowan ^e,
J. Fernandez ^d, J. Fuchs ^b, M. Geissel ^f, M. Hegelich ^d, S. Karsch ^g, H. Ruhl ^e,
M. Schollmeier ^a, R. Stephens ^h

^a Technische Universität Darmstadt, 64289 Darmstadt, Germany

^b Laboratoire pour l'Utilisation des Lasers Intenses, Palaiseau, France

^c Gesellschaft für Schwerionenforschung, 64291 Darmstadt, Germany

^d Los Alamos National Laboratory, Los Alamos, NM 87545, USA

^e Physics Department, MS-220, University of Nevada, Reno, NV 89557, USA

^f Sandia National Laboratory, Albuquerque, NM 87185, USA

^g Max-Planck-Institut für Quantenoptik, 85748 Garching, Germany

^h General Atomics, San Diego, CA 92121, USA

Received 28 October 2005; accepted 23 December 2005

Abstract

Intense lasers of femtosecond pulse duration are known to be drivers for intense electron and ion beams. Those beams, generated at laser intensities exceeding 10^{19} W/cm², are known to have unique characteristics and are therefore a subject of intense research world wide. Recently, the parameters of laser driven ion beams have been measured using new methods and it has been demonstrated, that beam patterns on a nanometer scale can be generated and propagated over long distances. We report on recent results and prospects for future application with special respect to further laser developments.

© 2006 Elsevier B.V. All rights reserved.

1. Introduction

The advent of high energy short pulse lasers has triggered a wealth of new phenomena, ranging from laser induced nuclear transmutation [1], the creation of antimatter by infrared light, bursts of X-rays and neutrons with unprecedented peak brilliance [2] to the emission of electron beams of highest peak currents. Among those new phenomena, the observation of intense, directed, energetic beams of ions [3–5] has attracted much attention over the last years and is intensively investigated at almost all major laser facilities world wide. The interest has risen, not only because of the unmatched intensities and beam parameters as will be shown in this report, but also because of the number of applications

being envisioned from fundamental research [6–8], industrial application to medical treatment possibilities.

The crucial beam parameter for most of the applications is the beam quality, in the sense of the phase space occupied by the bunch of emitted ions. The smaller the longitudinal and transverse beam emittance, the phase space, at a given number of particles, the higher the beam quality and the higher the achievable peak brilliance. In this paper, we report on recent experimental results not only demonstrating lowest emittance characteristics, but also a technique imprinting nano-scale structures onto the ion beam.

The acceleration mechanism is known as target normal sheath acceleration (TNSA) and has been published in detail in [9,10]: In typical experiments thin foils irradiated by ultra-intense laser beams at intensities of the order of 10^{19} W/cm² generate intense bursts of ions off the rear surface, propagating normal to the rear surface orientation. It

* Corresponding author. Tel.: +49 615 116 5417; fax: +49 615 116 4321.
E-mail address: m.roth@gsi.de (M. Roth).

is common understanding that the high laminarity, or low emittance, of these beams stems from the fact that the acceleration process takes place on the rear, non-irradiated surface of the target. There, a dense, relativistic electron sheath is formed by the laser-accelerated electrons that have propagated through the target. The sheath produces an electrostatic field $>10^{12}$ V/m that ionizes the surface atoms almost instantaneously, forming a ~ 1 nm thick ion layer which, together with the electron sheath, resembles a virtual cathode [11].

There are other mechanism, which also produce forward-accelerated ions, although in lower numbers and at lower energies [12]. Protons, having the largest charge-to-mass ratio and originating from target surface contamination (water vapor and hydrocarbons), are preferentially accelerated in favor of heavier ions over a distance of a few microns, and up to tens of MeV. In typical experiments this forms a collimated beam with an approximately Boltzmann energy distribution at $kT = 5\text{--}6$ MeV. The extremely strong, transient acceleration taking place from an initially cold, unperturbed surface, results in the low beam emittance that seems to be limited only by the collisions with the co-moving electrons during the acceleration.

The transport of relativistic electrons through the target is an intensively studied research area because of its relevance not only for ion acceleration, but especially for the concept of fast ignition in inertial confinement fusion [13,14]. The transport of large currents through the target, the problem of beam filamentation, and the dependence on the target conductivity (with respect to the onset of return currents) are essential for a detailed understanding of the ion acceleration. One crucial parameter for the electron transport has been found to be the target conductivity [15]. Anomalous stopping has been investigated experimentally and theoretically using plastic and metal targets [16]. In the experiments special care must be taken to avoid extensive pre-pulses or large amounts of amplified spontaneous emission (ASE). The preceding ASE launches a shock wave into the target altering the initial conditions via shock wave heating thereby changing the target density and resistivity.

We find that given a smooth laser intensity profile, the electron transport can remain highly uniform through $50\ \mu\text{m}$ gold foils, but the introduction of insulating layers with thickness $>0.1\ \mu\text{m}$ [17,18] causes the onset of spatial modulation or disruption of the electron flow. This suggests that the initial cold-matter electrical properties and material interfaces are important [19], in agreement with new, more realistic PIC simulations. We also show that the electron sheath can be imprinted by the laser focal pattern. Thus target composition and laser imprint must be seriously considered as possible origins of spatially non-uniform transport observed in past experiments [20].

2. Experiments

A typical experimental setup is depicted in Fig. 1. An ultra-intense laser (100 TW typically) is focused by an off

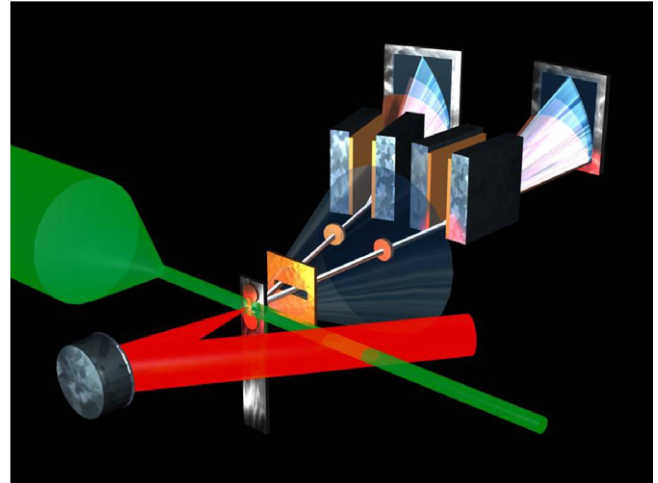


Fig. 1. Experimental setup. The ultra-intense laser (red) is focused by an off-axis parabola onto the free standing target. A stack of particle detectors (RCF or CR-39) is placed behind the thin target foil. A slit in the stack allows for a free line of sight to the spectrometers (Thompson parabolas), where the parallel electric and magnetic fields deflect the ions onto parabolic traces according to their energy and charge-to-mass ratio. A frequency up-converted laser is used (green) to monitor the plasma conditions of the target.

axis parabola onto a free standing target foil of millimeter size and a thickness of a few microns. It is mandatory for the efficiency of the TNSA mechanism for the rear surface to maintain cold, e.g. without any density gradient as might be caused due to the breakout of a pre-pulse induced shock wave. To monitor the initial conditions a frequency converted laser interferometer is used to measure any plasma gradients. The main ion beam diagnostics consists of a number of particle detectors like ion spectrometers or Thompson parabolas to separate different ion species [21]. The observation of any spatial beam structures and the measurement of the transverse beam emittance is done either by CR-39 nuclear track detectors or Radiochromic Film (RCF) detectors. In CR-39 ions above a few hundred keV of energy cause lattice damage on impact, which is etched in sodium hydroxide and visually examined under a microscope. This allows for single particle detection to obtain absolute numbers. For high particle numbers RCF films were used. In those detectors dye layers, exposed to ionizing radiation are changing color from transparent to dark blue according to the amount of deposited energy. Initially designed for X-rays we have absolutely calibrated the RCF for protons. Stacking multiple layers of CR-39 or RCF allows for a rough energy resolution due to the pronounced energy deposition of ions at the end of their range (Bragg peak). Because of the different energy deposition profiles and the much more pronounced deposition of energy by the impact of ions a clear distinction between ions and secondary radiation (electrons, X-rays) can be made.

For metal targets the electron transport seems to be extremely smooth and the resulting ion beams reveal a high quality. Details about the beam emittance and dependence

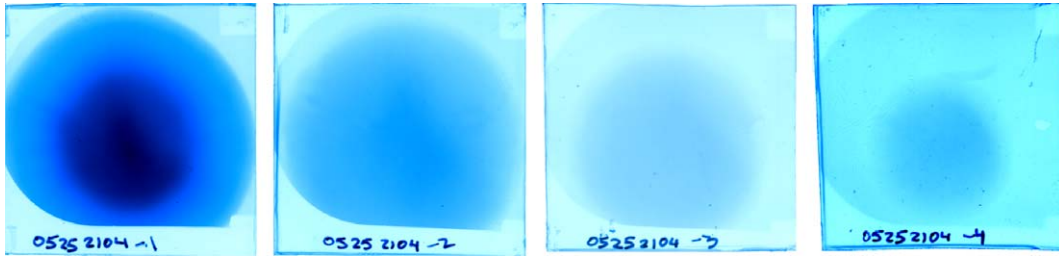


Fig. 2. Imprint of a laser accelerated proton beam, measured by a stack of RCF. The deeper the layer, the higher the energy of the stopped ions. The strength of the color is proportional to the number of particles. At higher energies the transverse beam size is reduced. The detectors show a homogenous beam of excellent quality (Note that the image on the right has been intensified to better visualize the ion beam).

from the initial conditions were published in [18,22], but it is worth to note that the measured emittance is at least a factor of 100–1000 better compared to ion beams from conventional accelerators. A typical example is shown in Fig. 2. In this figure, the proton beam reveals no internal structure. The homogenous intensity distribution indicates almost perfect beam properties.

3. Results

As stated before, the quality of charged-particle beams is characterized by their emittance, which is proportional to the volume of the bounding ellipsoid of the distribution of particles in phase space. By Liouville's theorem, the phase space volume of a particle ensemble is conserved during non-dissipative acceleration and focusing. For the transverse phase-space dimensions (e.g. $x - p_x$ for beam propagation along z), the area of the bounding phase-space ellipse equals $\pi\epsilon$, where the emittance ϵ , at a specific beam energy (or momentum p), is expressed in normalized root-mean square (rms) units as

$$\epsilon_{N,rms} = (|p|/mc) \left[\langle x^2 \rangle \langle x'^2 \rangle - \langle xx' \rangle^2 \right]^{1/2}$$

In this equation, m is the ion mass, c is the velocity of light, x is the particle position within the beam envelope and $x' = p_x/p_z$ is the particle's divergence in the x -direction. At a beam waist, this equation reduces to $\epsilon_{N,rms} = \beta\gamma\sigma_x\sigma_{x'}$, where σ_x and $\sigma_{x'}$ are the rms values of the beam width and divergence angle. Several effects contribute to the overall emittance of a beam: its intrinsic transverse 'thermal' spread; intra-beam space charge forces; and non-ideal accelerating fields, for example at apertures in the source or accelerator. For typical proton accelerators (e.g. the CERN SPS or FNAL-Tevatron), the emittance at the proton source is ~ 0.5 mm mrad (normalized-rms) and up to 20–80 mm mrad within the synchrotron. The longitudinal phase-space ($z - p_z$) is characterized by the equivalent, energy-time product of the beam envelope and a typical value, for the CERN SPS, is ~ 0.1 eV s. The highest quality ion beams have the lowest values of transverse and longitudinal emittance, indicating a low effective ion temperature and a high degree of angle-space and time-energy correlation.

Our measured upper limit of the emittance for 12 MeV protons was < 0.002 mm mrad [22]. This is a factor of > 100 smaller than typical proton beam sources, which we attribute to the fact that during much of the acceleration the proton space charge is neutralized by the co-moving hot electrons, and that the sheath electric field self-consistently evolves with the ions to produce an effectively 'ideal' accelerating structure.

Again it is important to note that a high target conductivity is mandatory for the homogeneity of the ion beam. This is caused by the need for return currents to flow in order to compensate for the huge magnetic field associated with the forward moving fast electron currents. If absent or suppressed by isolating layers the electron beam immediately starts to filament and consequently the ion acceleration is split into filaments, too [6]. Once given a laminar electron sheath at the rear surface the ion beam quality is that excellent, that even target surface structures of nanometer size can be imaged onto distant detector systems.

To demonstrate the high quality of the ion beam we designed special targets, where only the rear, non-irradiated surface was structured in order to produce a fiducial beam pattern. Figs. 3 and 4 show some of the target surface images measured with scanning electron or atomic force microscopy. Moreover in Figs. 3 and 4 examples of the resulting proton beams originating from these surfaces are shown.

Fig. 3 clearly demonstrates the excellent quality of the ion beam that allows for direct imaging the rear surface. This one to one correlation between a point at the surface to the point at the detector plane allows for the precise measurement of the source size of the ion beam, the beam emittance on divergence angle for each particle energy.

Fig. 4 shows that structures of only a few 100 nm in depth could be detected by the proton beam accelerated from this surface. The highest lateral resolution we found in our experiments so far (still detector limited) was of the order of 250 nm on the surface. In initial ion beam density modulation caused by the surface structure are being preserved by the laminarity of the beam and by with the help of the co-moving electrons that compensate for space charge and current effects.

Having been able to precisely tailor target surfaces for those experiments we also have measured the source size

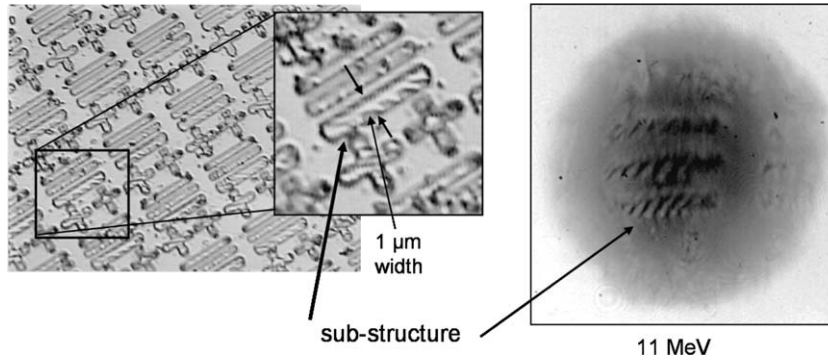


Fig. 3. Left: image of the rear, non-irradiated target surface with a test pattern imprinted by electron lithography. The inset on the left shows a magnified part including a sub-structure of less than 1 μm in size, caused by the electron beam. The right part of the figure shows the proton beam pattern in RCF at several centimeters of distance at an energy of 11 MeV. The sub-structure is clearly visible in the ion beam.

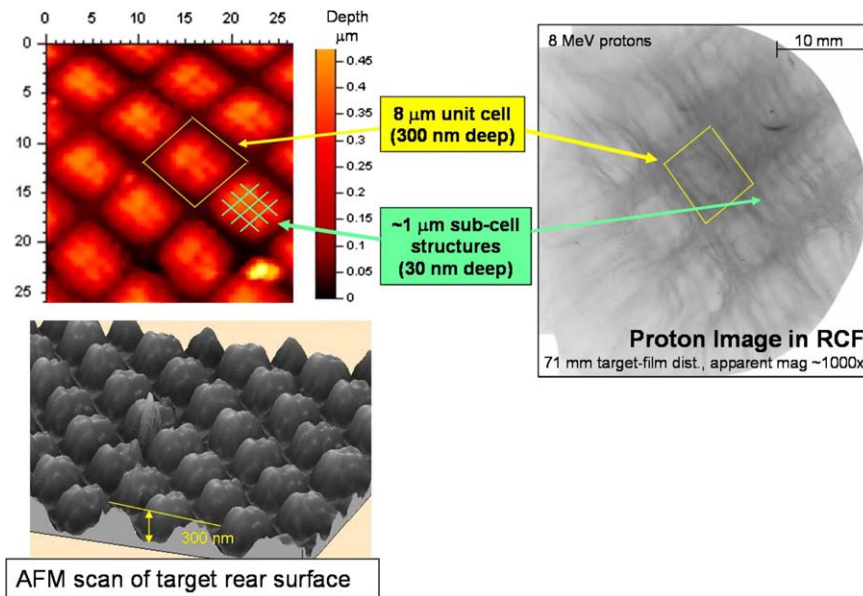


Fig. 4. Left: rear surface structure of a gold target. Superimposed onto the 8 μm unit cell structure of 300 nm depth there is a 1 μm sub-structure of only 30 nm depth, which is also visible in the 8 MeV proton beam detected by RCF on the right part of the figure.

of the proton beam for different energies, thereby mapping the initial electron density distribution as shown in Fig. 5.

The mechanism of the pattern formation has been explained in detail in [11]. The image generation basically consists of two steps. The initial perturbation in momentum space, triggered by the corrugated surface is followed by the expanding flow, both driven by the electric field caused by the electron pressure. The electron pressure expands the flow to a point where the divergence angles of the perturbations are well separated from each other, thus forming an image at even distant detectors. From the theoretical background and also supported by computer simulations a smooth parabolic or sinusoidal structure on the surface should result in the highest contrast by local microfocusing of the individual ion beamlets. A corresponding target surface is shown in Fig. 6, where on the rear surface of a 50 μm gold foil a number of concave grooves have been engraved.

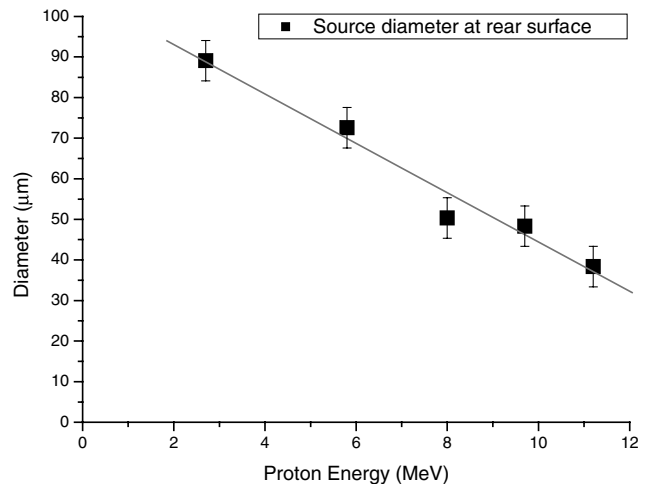


Fig. 5. One real source size measurement on the target surface based on the measurements of the beam structure. Note that the laser focal spot on the front surface is only of about 5 μm in size.

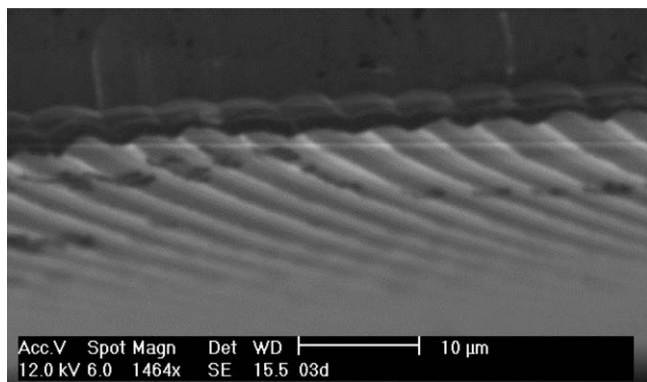


Fig. 6. SEM image of the rear surface of a gold foil with imprinted concave structures to produce high contrast ion beam patterns.

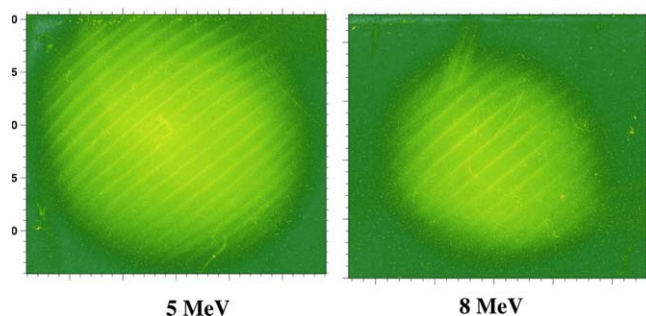


Fig. 7. Laser accelerated proton beams at 5 and 8 MeV respectively. The structure of the target rear surface is clearly imprinted in the beam. Slight distortions in the initially straight grooves can be observed in the image.

The ion beam patterns obtained from those surface structures are shown in Fig. 7, where an excellent reproduction of the initial grating pattern can be seen. The applications of those patterned beams are numerous, ranging from fiducial beam structures in modern dense plasma diagnostics to ion beam lithography or simply the investigation of intense electron beam propagation through targets that ultimately cause the onset of the accelerating sheath.

It is interesting to note that slight distortions of the initially straight grooves on the target rear surface can be observed in the image. This phenomenon has been observed in experiments at different laser systems. We believe the origin for this distortion to be a slight deviation of the accelerating electron density distribution from an ideal one. Details about the dependence of the image distortions to the initial electron distribution are published in [23].

4. Conclusion and outlook

So far the acceleration of ions by ultra-intense lasers has demonstrated beam properties of unrivaled excellence. The maximum energy of the particle distribution and the conversion efficiency has been correlated to the maximum power and total energy of the laser driver. We have demonstrated the use of micro-structured targets to imprint these local perturbations into the transverse density distribution

of the accelerated ions. This technique allows for the tailoring of the ion beams on a nanometer scale, but also serves as a superior diagnostic. Crucial parameters like divergence, source size and hence emittance can be measured with unprecedented accuracy. Most of the current ultra high intensity laser systems are limited by the damage threshold of the last of the gratings needed for temporal pulse re-compression. This is due to the low damage threshold of gold gratings available today. Over the last years efforts have been made to investigate the laser-induced breakdown in dielectrics for pulse length of picosecond to femtosecond time scales [24]. As a result of those studies the idea of dielectric, large scale diffraction gratings with high damage thresholds has emerged [25]. New facilities using this new technology will be able to extend the presently achievable beam parameters to even higher energies (beyond 100 MeV) and to higher conversion efficiencies (exceeding 10%), while preserving the beam quality with tailoring on a nano-scale to open up new frontiers in beam matter interaction.

Acknowledgements

We acknowledge the expert support of the LULI, RAL and Trident laser teams. This work was supported by Grant E1127 from Région Ile-de-France, EU program HPRI CT 1999-0052, LANL Laboratory Directed Research & Development, corporate support of General Atomics and UNR Grant DEFC08-01NV14050. Part of this work was performed within the Virtual Institute VIPBUL, funded by the Helmholtz Foundation.

References

- [1] K.W.D. Ledingham, P. McKenna, R.P. Singhal, *Science* 300 (2003) 1107.
- [2] J.M. Yang, P. McKenna, K.W.D. Ledingham, T. McCanny, L. Robson, S. Shimizu, R.P. Singhal, M.S. Wei, K. Krushelnick, R.J. Clarke, D. Neely, P.A. Norreys, *J. Appl. Phys.* 96 (2004) 6912.
- [3] R.A. Snavely, M.H. Key, S.P. Hatchett, T.E. Cowan, M. Roth, T.W. Phillips, M.A. Stoyer, E.A. Henry, T.C. Sangster, M.S. Singh, S.C. Wilks, A. MacKinnon, A. Offenberger, D.M. Pennington, K. Yasuike, A.B. Langdon, B.F. Lasinski, J. Johnson, M.D. Perry, E.M. Campbell, *Phys. Rev. Lett.* 85 (14) (2000) 2945.
- [4] E.L. Clark, K. Krushelnick, M. Zepf, F.N. Beg, M. Tatarakis, A. Machacek, M.I.K. Santala, I. Watts, P.A. Norreys, A.E. Dangor, *Phys. Rev. Lett.* 85 (2000) 1654.
- [5] A. Maksimchuk, S. Gu, K. Flippo, D. Umstadter, V.Y. Bychenkov, *Phys. Rev. Lett.* 84 (2000) 4108.
- [6] M. Roth, A. Blazevic, M. Geissel, T. Schlegel, T.E. Cowan, M. Allen, P. Audebert, J. Fuchs, J.-C. Gauthier, J. Meyer-ter-Vehn, M. Hegelich, S. Karsch, A. Pukhov, *Phys. Rev. ST-AB* 5 (2002) 061301.
- [7] M. Borghesi, D.H. Campbell, A. Schiavi, O. Willi, A.J. MacKinnon, D. Hicks, P. Patel, L.A. Gizzi, M. Galimberti, R.J. Clarke, *Laser Part. Beams* 20 (2002) 269.
- [8] M. Roth, T.E. Cowan, M.H. Key, S.P. Hatchett, C. Brown, W. Fountain, J. Johnson, D.M. Pennington, R.A. Snavely, S.C. Wilks, K. Yasuike, H. Ruhl, F. Pegoraro, S.V. Bulanov, E.M. Campbell, M.D. Perry, H. Powell, *Phys. Rev. Lett.* 86 (2001) 436.
- [9] S. Hatchett, C. Brown, T.E. Cowan, E.A. Henry, J. Johnson, M.H. Key, J.A. Koch, A.B. Langdon, B.F. Lasinski, R.W. Lee, A.J.

- MacKinnon, D.M. Pennington, M.D. Perry, T.W. Philips, M. Roth, T.C. Snangster, M.S. Singh, R.A. Snavelly, M.A. Stoyer, S.C. Wilks, K. Yazuhike, *Phys. Plasmas* 7 (5) (2000) 2076.
- [10] S.C. Wilks, A.B. Langdon, T.E. Cowan, M. Roth, M. Singh, S. Hatchett, M.H. Key, D. Pennington, A. MacKinnon, R.A. Snavelly, *Phys. Plasmas* 8 (February) (2001) 542.
- [11] H. Ruhl, T.E. Cowan, J. Fuchs, *Phys. Plasmas* 11 (2004) L17.
- [12] J. Fuchs, Y. Sentoku, S. Karsch, J. Cobble, P. Audebert, A. Nikroo, P. Antici, E. Brambrink, A. Blazevic, E.M. Campbell, J.-C. Gauthier, M. Geissel, M. Hegelich, H. Pepin, H. Popescu, N. Renard-LeGalloudec, M. Roth, J. Schreiber, R. Stephens, T.E. Cowan, *Phys. Rev. Lett.* 94 (05) (2005) 045004.
- [13] J.J. Honrubia, A. Antonicci, D. Moreno, *Laser Part. Beams* 22 (2004) 129.
- [14] C. Deutsch, *Laser Part. Beams* 22 (2004) 115.
- [15] K.B. Wharton, S.P. Hatchett, S.C. Wilks, M.H. Key, J.D. Moody, V. Yanovsky, A.A. Offenberger, B.A. Hammel, M.D. Perry, C. Joshi, *Phys. Rev. Lett.* 81 (1998) 822.
- [16] F. Pisani, A. Bernadinello, D. Batani, A. Antonicci, E. Martinolli, M. Koenig, L. Gremillet, F. Amiranoff, S. Baton, J. Davies, T. Hall, D. Scott, P. Norreys, A. Djaoui, C. Rousseaux, P. Fews, H. Bandulet, H. Pepin, *Phys. Rev. E* 62 (2000) R5927.
- [17] M. Roth, M. Allen, P. Audebert, A. Blazevic, E. Brambrink, T.E. Cowan, J. Fuchs, J.-C. Gauthier, M. Geissel, M. Hegelich, S. Karsch, J. Meyer-ter-Vehn, H. Ruhl, T. Schlegel, R.B. Stephens, *Plasma Phys. Contr. F.* 44 (2002) B99.
- [18] J. Fuchs, T.E. Cowan, P. Audebert, H. Ruhl, L. Gremillet, A. Kemp, M. Allen, A. Blazevic, J.-C. Gauthier, M. Geissel, M. Hegelich, S. Karsch, P. Parks, M. Roth, Y. Sentoku, R. Stephens, E.M. Campbell, *Phys. Rev. Lett.* 91 (2003) 255002.
- [19] S.I. Krasheninnikov, A.V. Kim, B.K. Frolov, R. Stephens, *Phys. Plasmas* 12 (2005) 073105.
- [20] R. Kodama, K. Mima, K.A. Tanaka, Y. Kitagawa, H. Fujita, K. Takahashi, A. Sunahara, K. Fujita, H. Habara, T. Jitsuno, Y. Sentoku, T. Matsushita, T. Miyakoshi, N. Miyanaga, T. Norimatsu, H. Setoguchi, T. Sonomoto, M. Tanpo, Y. Toyama, T. Yamanaka, *Phys. Plasmas* 8 (2001) 2268.
- [21] M. Hegelich, S. Karsch, G. Pretzler, D. Habs, K. Witte, W. Guenther, M. Allen, A. Blazevic, J. Fuchs, J.-C. Gauthier, M. Geissel, P. Audebert, T.E. Cowan, M. Roth, *Phys. Rev. Lett.* 89 (2002) 085002.
- [22] T.E. Cowan, J. Fuchs, H. Ruhl, A. Kemp, P. Audebert, M. Roth, R. Stephens, I. Barton, A. Blazevic, E. Brambrink, J. Cobble, J. Fernandez, J.-C. Gauthier, M. Geissel, M. Hegelich, J. Kaae, M. Karsch, G.P. Le Sage, S. Letzring, M. Manclossi, S. Meyroneinc, A. Newkirk, H. Pepin, N. Renard-LeGalloudec, *Phys. Rev. Lett.* 92 (2004) 204801.
- [23] E. Brambrink, M. Roth, A. Blazevic, T. Schlegel, *Laser Part. Beams* 24 (2006) 163.
- [24] B.C. Stuart, M.D. Feit, S. Herman, A.M. Rubenchik, B.W. Shore, M.D. Perry, *Phys. Rev. B* 53 (1996) 1749.
- [25] M.D. Perry, J.A. Britten, H.T. Nguyen, B.W. Shore, US Patent 5.907436, 1999.